JOURNAL OF MATERIALS RESEARCH AND TECHNOLOGY 2021;10:711–721

Available online at www.sciencedirect.com

jmr&t Journal of Materials Research and Technology

journal homepage: www.elsevier.com/locate/jmrt

Original Article

Exciplex-forming systems with extremely high RISC rates exceeding 10^7 s^{-1} for oxygen probing and white hybrid OLEDs

Malek Mahmoudi [a], *Jonas Keruckas* [a], *Karolis Leitonas* [a], *Stepan Kutsiy* [b], *Dmytro Volyniuk* [a,**], *Juozas V. Gražulevičius* [a,*]

[a] *Department of Polymer Chemistry and Technology, Kaunas University of Technology, Baršausko Str. 59, LT, 51423, Kaunas, Lithuania*

[b] *Department of Electronic Devices, Lviv Polytechnic National University, S. Bandera 12, 79013, Lviv, Ukraine*

ARTICLE INFO

Article history:
Received 6 October 2020
Accepted 18 December 2020
Available online 24 December 2020

Keywords:
Thermally activated delayed fluorescence
Organic-light-emitting diode
Optical sensor
Carbazole

ABSTRACT

A rare example of exciplex-forming systems with highly efficient thermally activated delayed fluorescence (TADF) exhibiting reverse intersystem crossing (RISC) yields of 97 and 96% and RISC rates of 5.1×10^7 and 3.6×10^7 s^{-1} at 300 K are developed for oxygen probing and organic light-emitting diodes (OLEDs). The exciplexes forming systems consist of a commercial acceptor 2,4,6-tris [3-(diphenylphosphinyl)phenyl]-1,3,5-triazine and a donor diphenyl bicarbazole substituted by electron withdrawing fluoro- or trifluoromethyl units. Affected by the donor modification, exciplex-forming system containing fluoro-substituted diphenyl bicarbazole demonstrated higher TADF efficiency due to its higher hole mobility ($\mu_h = 1.1 \cdot 10^{-3}$ $cm^2/V \cdot s$ at $1.6 \cdot 10^5$ V/cm) and lower activation energy (E_a) of 52 meV for exciplex formation in comparison to E_a of 127 meV observed for exciplex formation of trifluoromethyl-substituted diphenyl bicarbazole which is characterized by μ_h of $7.7 \cdot 10^{-5}$ cm^2/V at the same electric field. Due to extremely high RISC rates (one of the highest for TADF emitters observed up to now to the best of our knowledge), TADF was detected even under oxygen atmosphere. The developed exciplex emission based oxygen probes are characterised by non-linear oxygen sensitivity with the Stern–Volmer constants of ca. $3.27 \cdot 10^{-3}$ and 4.7 ppm^{-1}. In order to demonstrate possible OLED applications of the developed exciplex-forming systems, solution-processed white hybrid OLEDs with very high colour rendering index (CRI) of 92, colour temperature of 3655 K and CIE1931 coordinates of (0.384, 0.399) were fabricated using exciplex-forming emitters.

1. Introduction

Exciplex-forming organic donor–acceptor systems have big potential for electroluminescent devices such as organic-light-emitting diodes (OLEDs) and vertical light-emitting

* Corresponding author.
** Corresponding author.
E-mail addresses: dvolynyuk@gmail.com (D. Volyniuk), juozas.grazulevicius@ktu.lt (J.V. Gražulevičius).

https://doi.org/10.1016/j.jmrt.2020.12.058

transistors [1,2]. Particularly, big interest to exciplex emission is mainly grounded on:

- Possibility to harvest "dark" triplets via reverse intersystem crossing (RISC) of thermally activated delayed fluorescence (TADF) phenomenon; [3,4].
- Ability to decrease energy barriers for transported charges in device structures via formation of an "active" pn-heterojunction resulting in low turn-on voltage, thus high OLED power efficiency (exceeding of 100 l m/W); [5].
- Simplicity of obtaining of exciplex emission by mixing of electron donating and electron accepting molecules in solid state; [6].
- Versatility of different types of device structures since exciplex-forming systems are utilized as emitters, hosts, and they can be formed/transferred through relatively long distance; [7–10].
- Broad emission spectra and dual/multi-peak emission of exciplexes are suitable for realization of white OLEDs [11].

Among the best cases, exciplex emission characterized by very high reverse intersystem crossing (RISC) rates of 7.3×10^6 s^{-1} for TSBPA:POT2T [12] or 1.42×10^6 s^{-1} for DBT-SADF:PO-T2T:CDBP [13] was observed. It allowed to obtain exciplex emission based OLEDs with external quantum efficiency (EQE) higher than 20%. The abbreviation TSBPA is used for 4,4′-(diphenylsilanediyl)bis (N,N-diphenylaniline, PO-T2T is used for 2,4,6-tris [3-(diphenylphosphinyl)phenyl]-1,3,5-triazine, DBT-SADF is used for 2-(spiro [acridine-9,9′ -fluoren]-10-l)dibenzo [b,d]thiophene 5,5-dioxide, and CDBP is used for 4,4′-bis(9-carbazolyl)-2,2′-dimethylbiphenyl. Such RISC rates (k_{RISC}) observed for exciplex forming systems are comparable or even higher than RISC rates of state-of-art TADF emitters exhibiting k_{RISC} values of ca.10^6 s^{-1} [14,15]. However, TADF efficiencies of exciplex-based emitters are typically low at room temperature (RT) which affects EQE of electroluminescent devices. For instance, OLED based on exciplex-forming molecular mixture mMTDATA:3TPYMB exhibited lower EQE of 6.3% at RT than at 248 K (11%) [16]. Here, m-MTDATA is 4,4′,4″-tris [phenyl (m-tolyl)amino]triphenylamine and 3TPYMB is tris(2,4,6-trimethyl-3-(pyridin-3-yl)phenyl) borane. The similar observation was previously attributed to high non-radiative singlet and triplet transition rates (k_{nr}^S and k_{nr}^T, respectively) of exciplexes at room temperature [17]. It was concluded that not only high RISC rates but also low non-radiative transition rates are required for efficient exciplex based TADF [17].

In this work, we aimed to find out whether high k_{RISC} and high k_{RISC}/k_{nr}^T relation can be obtained for exciplexes when exciplex-forming donor diphenyl bicarbazole is modified by electron withdrawing fluoro- or trifluoromethyl units. 9,9-H or 9,9-diphenyl bicarbazole showed good performances in OLEDs as exciplex-forming donors [18–20]. We expected that substitution of diphenyl bicarbazole by acceptor units will result at least in higher ionization potentials compared to unsubstituted ones. Thus, knowing that the exciplex emission maximum wavelength can be described by formula $h\upsilon_{ex}^{max} \simeq I_D^D - E_A^A - E_C$, where I_D^D is the ionization potential of a donor, E_A^A is the electron affinity of an acceptor, and E_C is the electron–hole Coulombic attraction energy [21], we expected that the attachment of accepting moieties to diphenyl bicarbazole may result in the shift of emission of exciplexes to the higher-energy region. In addition, bipolar charge transport, which is required for functional OLED materials (e.g. for hosts and emitters), can be expected for compounds containing donor and acceptor units [22,23]. Taking into account these considerations, we synthesized two new diphenyl bicarbazoles (**bFPC** and **bTfPC** in Scheme 1). At RT, solid-state mixtures **bFPC**:PO-T2T and **bTfPC**:PO-T2T demonstrated efficient exciplex emission with the similar k_{RISC} of 5.1×10^7 and 3.6×10^7 s^{-1} but different k_{RISC}/k_{nr}^T of 1.1 and 0.27, respectively. Because of that, different photoluminescence quantum yields (PLQY) of 56 and 22% were recorded for exciplex-forming molecular mixtures **bFPC**:PO-T2T and **bTfPC**:PO-T2T, respectively. Despite extremely high k_{RISC} and relatively high k_{RISC}/k_{nr}^T their PLQYs were still much below 100%. Relatively low PLQYs can be explained by relatively low relationship of rates of prompt fluorescence to non-radiative singlet transition rates (k_{pr}/k_{nr}^S) of 41.4×10^{-3} observed for **bFPC**:PO-T2T and 10.5×10^{-3} recorded for **bTfPC**:PO-T2T. Thus, not only TADF efficiency but also efficiency of prompt fluorescence has to be increased for exciplex-forming systems. Nevertheless, having exciplexes with RISC yields of 97 and 96%, it is possible to employ them in optical sensors of oxygen. Naturally, quenching of TADF under presence of oxygen is expected. Several examples of TADF emitters were reported as active oxygen sensing materials [24,25] but to the best of our knowledge, the systems exhibiting exciplex based TADF were not yet used for this purpose. In addition, we used exciplex-forming molecular mixtures **bFPC**:PO-T2T and **bTfPC**:PO-T2T as green emitters in solution-processed hybrid white OLEDs based on polymeric host which acted also as a blue emitter doped by low concentration of a red phosphorescent emitter. Mixing blue fluorescence, green exciplex emission and red phosphorescence we achieved high colour rendering index (CRI) of 92, low correlated colour temperature of 3655 K and CIE1931 coordinates of (0.384, 0.399).

Originality of the proposed approach for the fabrication of white hybrid OLEDs is based on the distribution of electrical excitation energy between two light emitting layers, namely between green exciplex-based TADF and blue/red fluorescent/phosphorescent ones. The hole–electron recombination zone was mainly situated within the green exciplex-based light-emitting layer while part of electrical excitation energy was transferred to the blue/red emitting layer by direct hole–electron recombination and by exciton energy transfer. Such allocation of exciton energy resulted in relatively stable white emission under different external voltages.

2. Experimental

Materials. Molybdenum (VI) oxide (MoO_3), poly (9,9-dioctylfluorene-alt-N-(4-sec-butylphenyl)-diphenylamine) (TFB), bis(1-phenylisoquinoline) (acetylacetonate)iridium (III) (Ir (piq)$_2$ (acac)), 2,4,6-tris [3-(diphenylphosphinyl)phenyl]-1,3,5-triazine (PO-T2T), diphenyl-4-triphenylsilylphenyl-phosphine oxide (TSPO1), 2,2′,2″-(1,3,5-benzinetriyl)-tris(1-

phenyl-1-H-benzimidazole) (TPBi), and lithium fluoride (LiF) were purchased from Sigma–Aldrich or Lumtec companies and used without additional purification.

OLED fabrication. Electroluminescent devices with the structures of ITO/MoO_3/TFB:Ir $(piq)_2$ (acac) (EML2)/**BFPC**:PO-T2T or **BTfPC**:PO-T2T (EML1)/TSPO1/TPBi/LiF:Al were fabricated by a spin-coating/evaporation hybrid method. Indium-tin-oxide (ITO)-coated substrates were consecutively cleaned in an ultra-sonic bath containing acetone solution, distilled water and treated by UV-ozone for 15 min. Then, the devices were prepared by step-by-step depositions of different organic layers. The first (EML1) (**BFPC**:PO-T2T or **BTfPC**:PO-T2T) and the second (EML2) (TFB:Ir $(piq)_2$ (acac)) light-emitting layers were spin-coated while the other layers were vacuum-evaporated. The layers EML1 and EML2 were deposited from toluene solutions (4 mg/ml) of the corresponding compound mixtures under inert gas atmosphere inside a glove box. After spin-coating of EML1 and EML2, the samples were thermally annealed at 90 °C for 30 min (in case of EML1) or 180 °C for 40 min (in case of EML2). The vacuum-evaporated layers (MoO_3, TSPO1, TPBi, LiF and Al) were prepared under the vacuum of 10^{-6} mBar. All of the vacuum-evaporated layers were deposited at a rate of 1 Å s^{-1} except the LiF layer which was deposited at 0.1 Å s^{-1}. The size of emissive pixel was of 6 mm^2.

Additional information on materials, instrumentation and device testing are presented in the Supplementary Information.

3. Results and discussion

3.1. *Synthesis and common characterizations*

Compounds **bFPC** and **bTfPC** were prepared by two-step synthetic procedure starting from 9*H*-carbazole as it is shown in Scheme 1. In the first step, carbazole was substituted at N-position by 4-fluorophenyl or 4-trifluoromethylphenyl groups using the respective aryl iodides under the modified Ullmann conditions [26]. The intermediate compounds **FPC** and **TfPC** were isolated by re-crystallization in good yields of ca. 70–90%. In the second step, the intermediates were coupled by oxidative method [27] using iron (III) chloride. The target compounds, 3,3′-bis [9-(4-fluorophenyl)carbazole] (**bFPC**) and 3,3′-bis [9-(4-trifluoromethylphenyl)carbazole] (**bTfPC**) were isolated after column chromatography and re-crystallization in sufficient yields of 67% and 52%, respectively (see ESI for the procedures).

While proceeding with our research, we have discovered more efficient synthetic procedure for **bFPC** compared to that reported by other authors [28]. Interestingly, the melting point of 86–88 °C reported for **bFPC** in ref. [28] is close to glass-transition temperature established by ourselves for this compound (Fig. 1a, Table 1). Thus, we assume that **bFPC** reported in ref. [28] was rather isolated as amorphous solid than crystalline material. However, the structural data for **bFPC** (NMR, IR, MS) well match with those reported previously.

Compounds **bFPC** and **bTfPC** were isolated as crystalline solids which was proved by their well-defined melting points (mp) (Table 1). The mp values for both materials were close and situate around 245 °C when measured in capillary (see ESI) and around 250 °C as established by DSC (sharp endothermic peaks in Fig. 1a, inset). Both the compounds formed molecular glasses with glass-transition temperatures (T_g) of 101 °C for **bFPC** and 111 °C for **bTfPC**. However, the glasses of these compounds tended to crystallize above their glass-transition temperatures (exothermic peaks at ca. 205 and 160 °C in Fig. 1a) and melted again at the same temperature as before.

According to the data of thermogravimetric analysis (TGA, Fig. 1a), five percent weight-loss temperatures established for **bFPC** and **bTfPC** were 374 and 350 °C, respectively. Since the compounds melted at 250 °C and their sample weights went down to zero even at not very high temperature (around 450 °C), the weight loss can be rather attributed to evaporation than to chemical decomposition.

In order to determine electrochemical energy levels of compounds **bFPC** and **bTfPC,** they were examined by cyclic voltammetry (CV). Their dichloromethane (DCM) solutions with tetra-*n*-butylammonium hexafluorophosphate ($TBAPF_6$) as supporting electrolyte showed oxidation half-waves with respect to ferrocene at 0.58 V for **bFPC** and 0.65 V for **bTfPC** (Fig. 1b, Table 1). Both compounds exhibited double reversible CV oxidation but no expressed reduction waves were observed for DCM solutions even when strong electron withdrawing CF_3 groups were present. Despite the small difference (0.07 V) between oxidation potentials of the solutions of **bFPC** and **bTfPC**, a noticeably bigger difference (0.26 eV) was observed between their ionization potentials estimated by photoelectron spectroscopy (PESA) in air. I_p^{PESA} of 5.78 eV was observed for the film of **bFPC** and 6.04 eV for the film of **bTfPC**(Fig. 1c inset, Table 1). I_p^{PESA} values of **bFPC** and **bTfPC** were found to be higher than corresponding values measured by CV. I_p^{CV} values of 5.38 and 5.45 eV respectively were recorded. Such discrepancy is typically observed due to the different physical meaning of I_p^{CV} and I_p^{PESA} [29]. Due to stronger electron accepting ability of CF_3 groups in comparison to that of F, the higher I_p^{PESA} (deeper HOMO) was obtained for compound **bTfPC** relative to that observed for **bFPC**.

Time of flight (TOF) experiment disclosed low-dispersity hole transport in the layers of **bFPC** and **bTfPC**. The transit times (t_{tr}) for holes were easily identified from TOF current transients at different external voltages (V) in log–log scales for the vacuum-deposited films (Fig. S1). Despite the presence of electron accepting fluoro- or trifluoromethyl substituents, electron transport ability was detected for the layers of **bFPC** and **bTfPC** by the TOF measurements (Fig. S1). Taking the t_{tr} values for holes at different external voltages, hole mobility (μ_h) at different electric fields (E) were calculated for **bFPC** and **bTfPC** (Fig. 1c). Dependences log (μ_h) versus $\sqrt{E}$ were well fitted by the Poole–Frenkel formula $\mu = \mu_0 e^{\alpha E^{1/2}}$ [30].

By the fitting, zero-field mobilities (μ_0) and field dependence parameter (α) were obtained. Slightly higher value of α observed for **bTfPC** was apparently due to its more dispersive charge transport**.** Higher by ca. 20 times μ_0 value observed for **bFPC** can apparently be explained by favourable molecular packing (Fig. 1c). Lower field dependence parameter α of $2.5 \cdot 10^{-3}$ cm/V was obtained for **bFPC** compared to that observed for **bTfPC** ($3.9 \cdot 10^{-3}$ cm/V) indicates lower charge dispersity in the layer of **bFPC** than in that of **bTfPC**.

Table 1 – Thermal, electrochemical, photoelectrical, hole-transporting and photophysical parameters of bFPC and bTfPC.

Property	Sample	bFPC	bTfPC
T_m, °C	Powder	246	253
T_g, °C		101	111
T_{cr}, °C		206	161
$T_{de\text{-}5\%}$, °C		374	350
$E_{ox\ vs\ Ag/Ag^+}$, V	DCM solution with $TBAPF_6$	0.58	0.65
IP_{CV}, eV		5.38	5.45
IP_{PE}, eV	Film	5.78	6.04
E_g^{opt}, eV		3.36	3.21
EA_{PE}, V		2.42	2.83
λ^{PL}, nm	Film (THF solution)	390, 409 (385[b], 402)	387, 404 (383[b], 397)
PLQY, %		19 (15)	15 (18)
τ, ns		4.68 (6.09)	4.02 (6.01)
E_{S1}^{THF}, eV	THF solution at 77 K	3.44	3.38
E_{T1}^{THF}, eV		2.99	2.99
ΔE_{S1T1}^{THF}, eV		0.45	0.39
μ_{holes},[a] $cm^2/(V\cdot s)$	Film	$1.1\cdot10^{-3}$	$7.7\cdot10^{-5}$

[a] At electric field of $1.6\cdot10^5$ V/cm.
[b] Shoulder.

Apparently, the presence of trifluoromethyl units hinders hoping of holes between HOMO–HOMO molecular orbitals of neighbouring molecules. In addition, more efficient formation of hydrogen bonds C–H···F in the layer of **bTfPC** than in the layer of **bFPC** can be the reason of the above described observations. The different values of hole mobility of **bFPC** and **bTfPC** might be also related to their molecular packing and/or different structure of the layers as it was proved for other carbazole-containing compounds [31]. Notably, μ_h of 1.1×10^{-3} $cm^2/V\cdot s$ recorded at electric field of 1.6×10^5 V/cm is by two orders of magnitude higher than hole mobility of efficient exciplex-forming bicarbazoles containing CN groups at the same electric fields (Table 1) [32,33]. In contrast to those CN-substituted bicarbazoles which showed bipolar charge

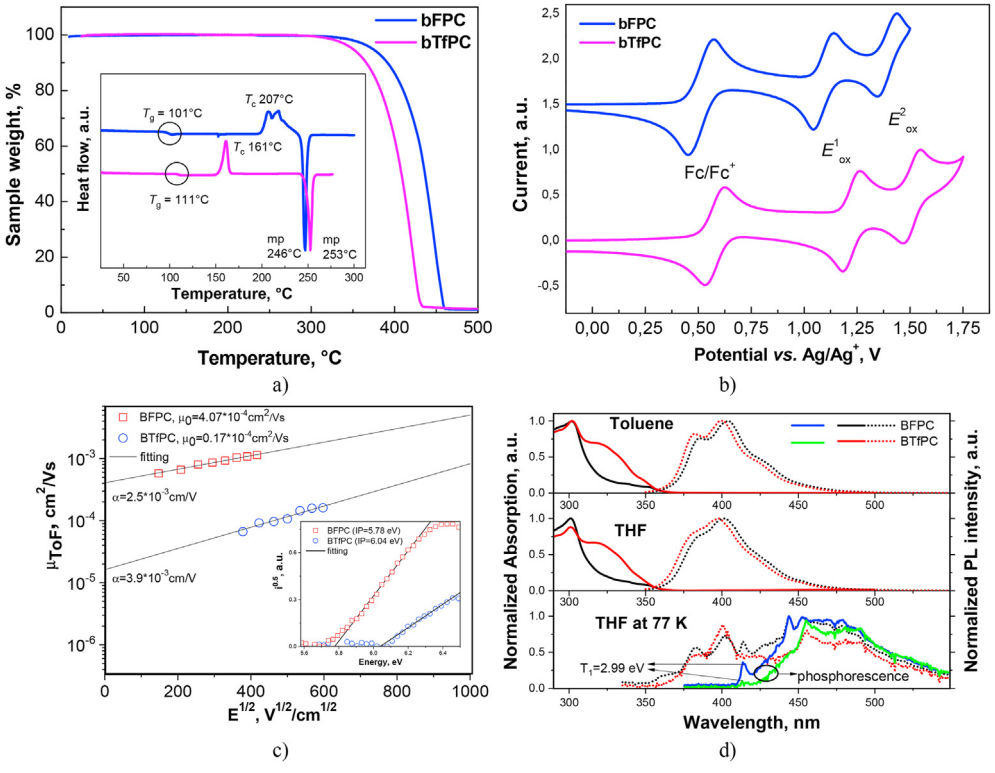

Fig. 1 – (a) DSC second heating scans (inset) and TGA curves; (b) CV voltammograms ("Fc" stands for ferrocene, $E^{ox}{}_1$ and $E^{ox}{}_2$ stand respectively for the first and the second oxidation waves); (c) hole mobility versus electric field and electron photoemission spectra (inset); (d) UV absorption, PL and phosphorescence spectra of the dilute solutions of bFPC and bTfPC. Phosphorescence spectra were recorded at 77 K with the delay of 50 ms after excitation turn-off.

transport, compounds **bFPC** and **bTfPC** exhibited only hole-transporting properties apparently because of the weak electron withdrawing ability of fluoro or trifluoromethyl units.

In order to investigate the effect of the different substituents on photophysical properties of the compounds, absorption and photoluminescent (PL) spectra of the dilute solutions (~10^{-5} M) of **bFPC** and **bTfPC** in toluene and THF were recorded (Fig. 1d). Carbazole unit is mainly responsible for absorption of the solutions of compound **bFPC** since the shape of its absorption spectrum is similar to that of carbazole, N-phenylcarbazole, and N,N′-diphenyl(-3,3-)bicarbazole [1,2,18]. The additional energy band around 325 nm can be recognized in the low-energy region of absorption spectra of the solutions of compound **bTfPC**. It was not observed in the spectra of the solutions of **bFPC** and N-phenylcarbazole [35]. The similar absorption band was observed for benzonitrile-substituted carbazole N-(4-cyanophenyl)carbazole (NP4CN) and was attributed to $S_0 \rightarrow$ charge transfer (CT) absorption [34]. Charge transfer between carbazole and trifluoromethylbenzene units induced that additional absorption band. Vibronically structured fluorescence spectra with two maxima at 385 and 405 nm were recorded for toluene solutions of **bFPC** and **bTfPC**. The similar fluorescence spectrum was previously reported for N-phenylcarbazoles and was attributed to locally exited (LE) emission (Fig. 1d) [34]. PL decays of the toluene solutions of the compounds were adequately represented by single-exponential fitting with the lifetimes of ca. 6 ns? The lifetimes slightly differed with the change of polarity of media (Fig. S2, Table S2). This effect is apparently related to different non-radiative rates of the compounds in different media. LE emission was also detected for the solutions of compounds **bFPC** and **bTfPC** in more polar TFH. A weak intramolecular CT (ICT) contribution can be recognised in the emission of compounds **bFPC** and **bTfPC** as it was shown for CF_3-substituted N-phenylcarbazole [35]. However, no any strong ICT emission was observed even for the films of compounds **bFPC** and **bTfPC**, as it was for reported for compound NP4CN with a relatively strong benzonitrile acceptor (Fig. 2a) [34]. Photoluminescence quantum yield (PLQY) values of the solutions and neat films of compounds **bFPC** and **bTfPC** (Table 1) are in agreement with PLQYs of the previously studied N-phenylcarbazoles and N-phenylbicarbazoles [18,33,35].

PL and phosphorescence spectra of THF solutions of **BFPC** and **BTfPC** were also recorded for getting their first excited singlet (E_{S1}) and triplet (E_{T1}) energy levels (taken from the first highest-energy peak) (Fig. 1d, Table 1). The compounds emit intense phosphorescence which is mainly related to the LE^3 emissive recombination of triplet state of carbazole moiety [36,37]. The differences observed in phosphorescence spectra of **bFPC** and **bTfPC** are apparently caused be weak influence of ICT^3 emission in case of **bTfPC**. Nevertheless, both compounds were characterized be the same energy of the first excited triplet states of 2.99 eV (Table 1).

3.2. *Exciplex-forming properties*

Compounds **bFPC** and **bTfPC** can be regarded as promising candidates as exciplex-forming donors for TADF emitters due to their high triplet levels, high hole mobilities, and fluorescence in near UV region. Indeed, solid-state mixtures **bFPC**:PO-T2T and **bTfPC**:PO-T2T demonstrated exciplex type emission which was typically red-shifted in comparison to pure emission of donor and acceptor compounds (Fig. 2a). PL

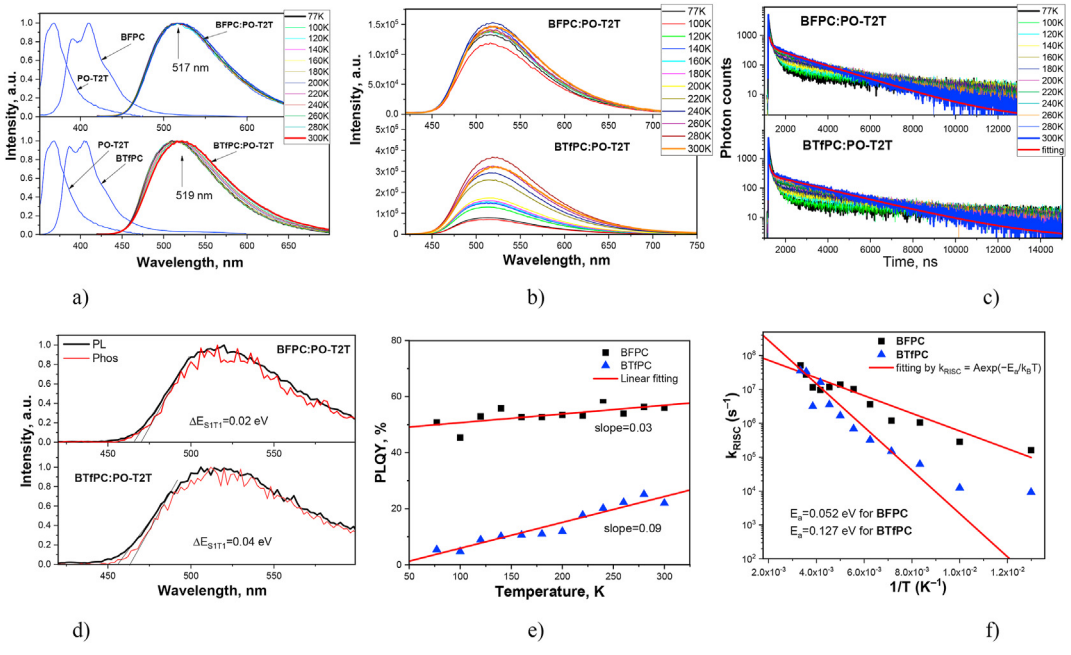

Fig. 2 – Normalized PL spectra (a) and intensity dependences on the temperature of PL spectra (b) of the films of bFPC, bTfPC, PO-T2T, bFPC:PO-T2T, and bTfPC:PO-T2T. The corresponding PL decay curves recorded at the indicated temperatures (c), PL and phosphorescence spectra recorded at 77K (d) of molecular mixtures bFPC:PO-T2T and bTfPC:PO-T2T. PLQY versus temperature (e) and k_{RISC} versus 1/T (f) plots for bFPC:PO-T2T and bTfPC:PO-T2T.

spectra of **bFPC**:PO-T2T and **bTfPC**:PO-T2T are peaked at the similar wavelength near 520 nm. Their PL decays were adequately fitted by double exponential law giving short-lived (τ_{PF} of 69–376 ns)) and long-lived ($\tau_{DF}$of 1.94–4.25 μs) components (Table 2). More than 90% of total emission intensity of exciplexes was related to delayed fluorescence which is thermally activated by nature. This statement was proved by the measurements of PL spectra and PL decays at the different temperatures (Fig. 2b,c). The presence of TADF is in the emission of the exciplex forming systems was confirmed by small singlet-triplet energy differences (ΔE_{S1T1}) which allowed RISC process and thus TADF (Fig. 2d) [4]. Having absolute PLQY values of exciplexes at RT and dependences od PL spectra on the temperature (Table 2, Fig. 2b), it was possible to plot PLQY versus temperature for exciplex emitters **bFPC**:PO-T2T and **bTfPC**:PO-T2T (Fig. 2e). In contrast to previously studied exciplexes which showed the highest efficiency at low temperatures [16,17], PLQY values of the studied exciplexes linearly increased with increasing temperature due to the efficient TADF and low non-radiative losses.

Solid molecular mixtures **bFPC**:PO-T2T and **bTfPC**:PO-T2T were also studied by the time-resolved luminescence spectrometry at the different temperatures (Tables 2 and S2) [4,5,38]. The values of prompt (η_{PF}) and delayed (η_{DF}) fluorescence quantum yields were obtained from PL decays fitting assuming that the total integral of PL transients is attributed to the absolute PLQYs of exciplexes **bFPC**:PO-T2T and **bTfPC**:PO-T2T (Table S2). Taking lifetimes of prompt and delayed fluorescence (τ_{PF} and τ_{DF}) and the corresponding quantum yields (η_{PF} and η_{DF}), radiative rates of prompt (k_{PF}) and delayed (k_{DF}) fluorescence were estimated (Tables 2 and S2). In addition, non-radiative rates of the singlet (k_{nr}^{S}) and triplet (k_{nr}^{T}) states were calculated. Non-radiative rate k_{nr}^{S} is mainly related to the intersystem crossing (ISC) with the quantum efficiency η_{ISC} and rate constant k_{ISC}. The RISC process is responsible for the population of the first singlet state (S1) resulting to the long-living component of PL transients. Rate constant k_{RISC} as a key parameter is generally attributed to efficient TADF and is in the order of 10^6 s^{-1} for state-of-art intramolecular and intermolecular TADF emitters [12–15]. Notably, exciplexes **bFPC**:PO-T2T and **bTfPC**:PO-T2T were characterized by extremely high k_{RISC} of 5.1×10^7 and 3.6×10^7 s^{-1} respectively, which are among the highest values to the best of our knowledge. Despite of the close k_{RISC} values, exciplex emission of **bFPC**:PO-T2T was found to be more efficient than emission of **bTfPC**:PO-T2T. The respective absolute PLQY values were found to be different, i.e. of 56% and 22% at room temperature (Table 2). This observation can be explained by the different non-radiative rate constants k_{nr}^{T} of 4.7×10^7 for **bFPC**:PO-T2T and of 1.35×10^8 for **bTfPC**:PO-T2T resulting in the different k_{RISC}/k_{nr}^{T} ratio of 1.1 and 0.27, respectively. Despite of the small difference in the molecular structures of compounds **bFPC** and **bTfPC** which practically have no effects on the exciplex emission spectra of **bFPC**:PO-T2T and **bTfPC**:PO-T2T, the different non-radiative rate constants k_{nr}^{T} were obtained for these exciplexes.

This observation may be attributed to the different molecular packing caused by the presence of the different fluoro- and trifluoromethyl substituents in **bFPC** and **bTfPC**. The presence of trifluoromethyl groups may be the reason of higher intermolecular distances in solid films leading to the higher non-radiative rate constant k_{nr}^{T} and to the less efficient

Table 2 – Photophysical parameters of exciplex-forming molecular mixtures bFPC:PO-T2T and bTfPC:PO-T2T derived at room temperature (300 K).

Exciplex	source/equation	bFPC: PO-T2T	bTfPC:PO-T2T
λ^{PL}_{max}, nm	taken from PL spectra	517	519
FWHM, nm		104	107
E_{S1}, eV	$E_{S1} = 1240/\lambda^{PL}_{seton}$	2.63	2.72
E_{T1}, eV	$E_{T1} = 1240/\lambda^{Phos}_{seton}$	2.64	2.68
ΔE_{S1T1}, eV	$\Delta E_{S1T1} = E_{S1}$-E_{T1}	0.02	0.04
PLQY, %	measured with a sphere	56	22
η_{PF}	$\eta_{PF} = \eta_{PLQY}$*PF(%)/100(%)	0.04	0.01
η_{ISC}	$\eta_{ISC} = 1$-η_{PF}	0.96	0.99
η_{DF}	η_{DF} = PLQY*DF(%)/100(%)	0.52	0.21
η_{RISC}	$\eta_{RISC} = \eta_{DF}/(\eta_{PLQY}*\eta_{ISC})$	0.97	0.96
E_a, eV	taken from k_{RISC} fitting by $k_{RISC} = A\exp(-Ea/k_BT)$	0.052	0.127
τ_{PF}, ns (%)	from PL decay fitting by I = A + B1exp (-t/τ_{PR})+B2exp (-t/τ_{DF})	110 (7)	94 (5)
τ_{DF}, μs (%)		1.94 (93)	2.47 (95)
τ_{PF}^{r}, μs	$\tau_{PF}^{r} = \tau_{PF}/\eta_{PF}$	2.8	9
τ_{PF}^{nr}, ns	$\tau_{PF}^{nr} = \tau_{PF}/(1-\eta_{PF})$	115	95
k_{PF}, s^{-1}	$k_{PF} = \frac{\eta_{PF}}{\tau_{PF}}$	3.6×10^5	1.1×10^5
k_{PF}^{r}, s^{-1}	$k_{PF}^{r} = 1/\tau_{PF}^{r}$	3.6×10^5	1.1×10^5
k_{nr}^{S}, s^{-1}	$k_{PF}^{nr} = 1/\tau_{PF}^{nr}$	8.7×10^6	1.05×10^7
k_{ISC}, s^{-1}	$k_{ISC} = \frac{\eta_{DF}}{\eta_{PF}+\eta_{DF}} k_{PF}$	0.25×10^5	0.05×10^5
k_{DF}, s^{-1}	$k_{DF} = \frac{\eta_{DF}}{\tau_{DF}}$	2.69×10^5	0.85×10^5
k_{RISC}, s^{-1}	$k_{RISC} = \frac{\eta_{DF}}{\eta_{PF}} \cdot \frac{k_{PF}.k_{DF}}{k_{ISC}}$	5.1×10^7	3.6×10^7
k_{nr}^{T}, s^{-1}	$k_{nr}^{T} = k_{RISC}/\eta_{RISC} - k_{RISC}$	4.7×10^7	1.35×10^8

TADF of **bTfPC**:PO-T2T in comparison to that of **bFPC:**PO-T2T. In case of exciplex formed by **bFPC**:PO-T2T, the lower non-radiative energy loss can be explained by a relatively large HOMO–LUMO orbital overlap since molecules of **bFPC** and PO-T2T in their solid molecular mixture are apparently closer to each other in comparison to distance between the molecules of **bTfPC** and PO-T2T in the solid molecular mixture. Thus, the different intermolecular distances between the molecules in the solid molecular mixtures of **bFPC**:PO-T2T and **bTfPC**:PO-T2T causing the different HOMO–LUMO overlaps apparently lead to the different radiative decay probabilities from excited spin-singlet states [11,12,32].

The different hole mobilities of **bFPC** and **bTfPC** have also to be taken into account. Since higher hole mobility of 1.1×10^{-3} $cm^2/V{\cdot}s$ was observed for compound **bFPC** (Fig. 1c, Table 1), it could be the reason of faster formation of hole–electron excited states (exciplexes). On the other, the probability of dissociation of hole–electron pairs into free charges may be increased for the exciplex **bFPC:**PO-T2T due to the high hole mobility of **bFPC** [12,32]. Free charges (positive and negative polarons) may lead to non-radiative energy loss of the exciplex states as it was concluded by the authors of ref. [32]. However, the authors of study [12] noted that formation of free charges not necessarily leads to the non-radiative energy loss of the exciplex states when the energy of local excited (LE) states of exciplex-forming compounds are above their CT exciplex states. It was presumed that "new" CT exciplex states could be formed by the dissociated free holes and electrons [12]. Despite the dissociation, when the triplet CT exciplex state lives long enough, efficient RISC can occur which is required for efficient TADF [12]. It is the case of exciplexes **bFPC**:PO-T2T and **bTfPC**:PO-T2T since their singlet and triplet LE states are higher than their CT exciplex states (Fig. 1 d, Tables 1 and 2). It shout be noted the faster formation of the "new" CT exciplex states from the dissociated charges is expected for the exciplex based on the compound **bFPC** with higher hole mobility in comparison to the **bTfPC**-based exciplex. Taking into account, the probability of dissociation of hole–electron pairs into free charges for both **bFPC**:PO-T2T and **bTfPC**:PO-T2T exciplexes, the lower non-radiative energy losses are expected for **bFPC**-based exciplex due to the fast formation of the "new" CT exciplex states followed by their emissive recombination.

Having k_{RISC} values at different temperatures, Arrhenius plots were plotted and fitted (in the range of T > 200K where phosphorescence is absent (limited)) according to Arrhenius equation: $k_{RISC} = A{\cdot}\exp(-E_a/k_BT)$, where A is the frequency factor involving the spin–orbit coupling constant, E_a is activation energy and k_B is Boltzmann constant [39]. By analysing the temperature dependences of k_{RISC}, E_a values of 0.052 and 0.127 eV were obtained for emission of exciplexes **bFPC:PO-T2T** and **bTfPC:PO-T2T**, respectively. These E_a values are in good agreement with their singlet-triplet splitting ΔE_{S1T1} allowing population of the emissive singlet exciplex state via RISC from the triplet exciplex state.

3.3. *Oxygen probing*

Exciplex-formig system **bFPC:PO-T2T** was selected for testing its applicability as oxygen probe. This system was characterized by higher total PLQY (56%) than BTfPC:PO-T2T (22%). Since exciplex emission of **bFPC:PO-T2T** was mainly characterized by delayed fluorescence (η_{DF}=52% versus η_{PF} = 4% (Table 2)), oxygen sensitivity of this system can be predicted if the delayed fluorescence is quenched under presence of oxygen (Table 2). This prediction is supported by the relation η_{DF}/η_{PF} = 13, which may be obtained from the relation of emission intensities estimated in the presence and in the absence of oxygen. Aiming to test exciplex-forming system **bFPC**:PO-T2T as active component for oxygen probing, three-component samples **bFPC**:PO-T2T:Zeonex (1:1:1) were fabricated. Zeonex 480 was used for the improvement of film-forming properties of the probe and for insuring oxygen permeability of the films [40]. PL spectra of the films of the mixtures **bFPC**:PO-T2T:Zeonex were recorded under different concentration of oxygen in constant flow of nitrogen:oxygen mixture when emission intensity was stabilized (Fig. 3a). Dependence of integrated emission intensity versus concentration of oxygen was then analysed by the Stern–Volmer equation which describes nonlinear curve: [41,42].

$$\frac{I_0}{I} = \frac{1}{\frac{f_1}{1+K_{SV1}[O_2]} + \frac{f_2}{1+K_{SV2}[O_2]}}, \quad (1)$$

where I_0 and I are emission intensities under nitrogen and at the different concentrations of oxygen; f_1 and f_2 are fractional contributions of different sensing sites; K_{SV1} and K_{SV2} are Stern–Volmer constants. The results of fitting are collected in the inset Table of Fig. 3b. The fitting with relatively high accuracy (R^2 = 0.9652) was performed using formula (1). The fitting data can be used for determination of specific concentration of oxygen measuring ratiometric properties of the samples of the mixtures **bFPC**:PO-T2T:Zeonex. Despite the

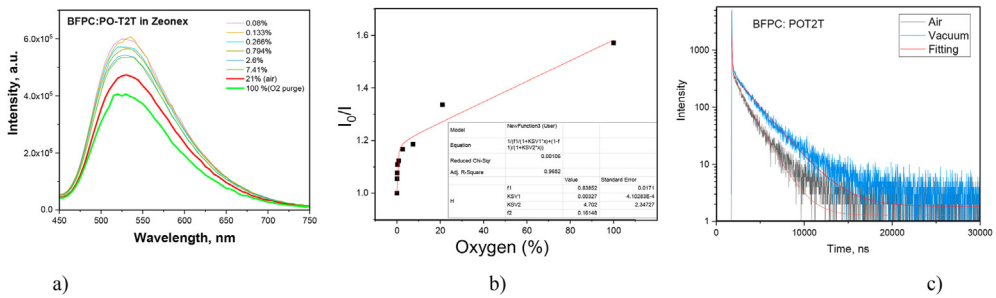

Fig. 3 – PL spectra (a), Stern–Volmer dependence (b), and PL decays (c) of the films of bFPC:PO-T2T:Zeonex under different concentration of oxygen.

high ratio η_{DF}/η_{PF} of 13, the ratio of emission intensity under pure nitrogen and emission intensity under pure oxygen ($I_{0\ [100\%\ N2]}/I_{[100\%\ O2]}$) of 1.57 was obtained which indicates relatively low oxygen sensitivity of the mixture **bFPC**:PO-T2T:Zeonex. This observation is in agreement with the results of PL decay measurements of the films of **bFPC**:PO-T2T:Zeonex under vacuum and under air demonstrating that this exciplex-forming system is characterized by delayed fluorescence even in the presence of oxygen. Apparently, delayed fluorescence cannot be totally quenched by oxygen when TADF emitters are characterized by extremely high k_{RISC}, which exceeds 10^7 s^{-1} (Table 2).

3.4. *Solution processed white hybrid organic light-emitting diodes*

Taking into account the green TADF with broad PL spectra of the studied exciplex-forming systems **bFPC:PO-T2T** and **bTfPC:PO-T2T**, they can be regarded as good candidates for getting white electroluminescence (EL) in combination with appropriate blue and red emitters. Blue emitting poly (9,9-dioctylfluorene-alt-N-(4-sec-butylphenyl)-diphenylamine) (TFB) [43] and red emitting bis(1-phenylisoquinoline) (acetylacetonate)iridium (III) (Ir (piq)$_2$ (acac)) [44] emitters were selected as one possible set of emitters which may enable to obtain natural white emission mixing their emission with the green exciplex emission of **bFPC:PO-T2T** and **bTfPC:PO-T2T** (Fig. 4a). The total spectrum (Fig. 4, orange line) obtained by mixing three emission spectra of TFB, **bFPC:PO-T2T** (or **bTfPC:PO-T2T**) and Ir (piq)$_2$ (acac) covers the whole visible region. This observation confirmed that the combinations of red, green, and blue emitters were well selected. The polymeric material TFB was selected aiming to fabricate partly solution processable white OLEDs. In addition to practical interest in solution-processing [45], this solution-based method allows precise control of concentration of an emitter in doped light-emitting layers which are required for the fabrication of white OLEDs. To get white electroluminescence, the device structure ITO/MoO_3 (1 nm)/TFB:Ir (piq)$_2$ (acac) (2, 5 or 10 wt%, 30 nm)/**bFPC**:PO-T2T (for the devices named as A2, A5 and A10, respectively) or **bTfPC**:PO-T2T (for the devices named as B2, B5 and B10, respectively) (1:1) (20 nm)/TSPO1 (8 nm)/TPBi (40 nm)/LiF:Al was selected, where the layer of MoO_3 was employed as hole injection layer, the layer of diphenyl-4-triphenylsilylphenyl-phosphine oxide (TSPO1) acted as hole/exciton blocking layer, the layer of 2,2′,2′′-(1,3,5-benzinetriyl)-tris(1-phenyl-1-H-benzimidazole) (TPBi) acted as electron transporting layer, and the layer of LiF acted as electron injection layer. The effect of concentration of the red phosphorescent emitter Ir (piq)$_2$ (acac) on the quality of white electroluminescence was investigated for devices A (A2, A5 and A10) and B (B2, B5 and B10), with the concentration of Ir (piq)$_2$ (acac) of 2, 5 and 10% respectively (Table 2). Such concentrations of the dopant in light-emitting layers based on the host-guest system were simply attainable because the layers were fabricated by spin-coating method.

Analysis of the equilibrium energy diagram of the device structures (Fig. 4b) revealed that the recombination zone of

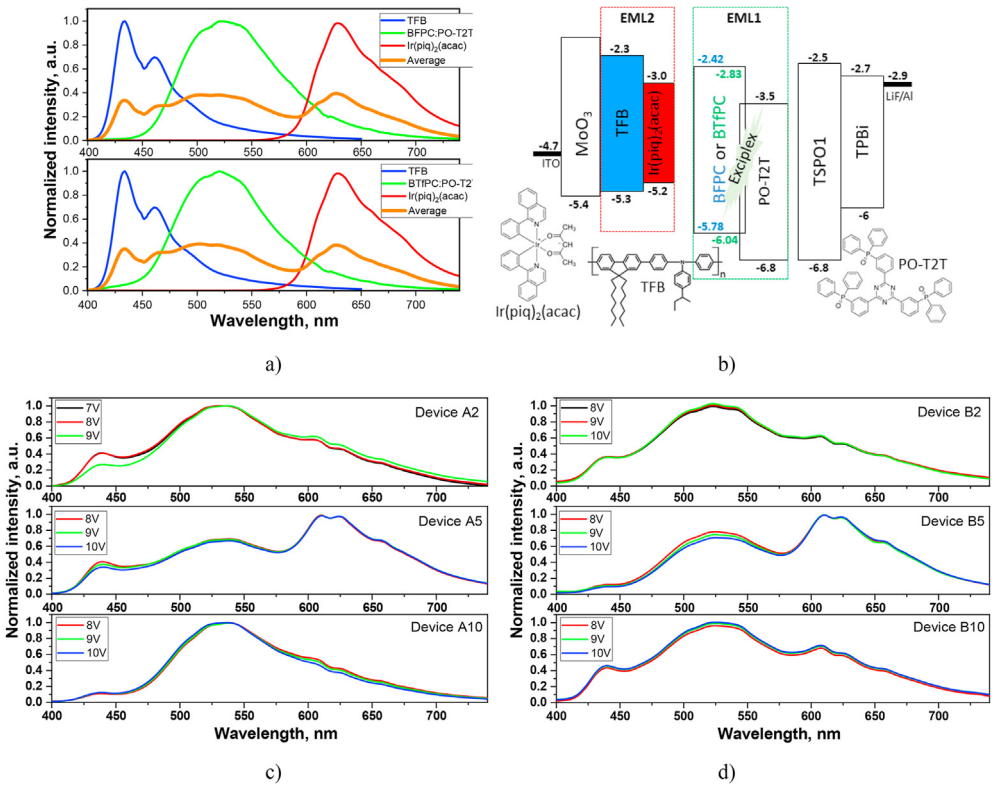

Fig. 4 – PL spectra of blue emitting TFB, green emitting bFPC:PO-T2T or bTfPC:PO-T2T, and red emitting Ir (piq)$_2$ (acac) and the total spectrum of the three emitters (a); visualized device structure with indication of energy levels of all functional layers (b); normalized electroluminescence spectra under different applied voltages for white bFPC:PO-T2T (c) and bTfPC:PO-T2T (d) based devices.

Table 3 – Electroluminescent parameters of white OLEDs.

Device	Emissive layers	V_{on},[a] (V)	Max. brightness, cd/m^2[b]	CE_{max},cd/A[c]	EQE_{max}, %[d]	CIE (x; y)[e]	CRI[f]	T_C, K[g]
A2	TFB:Ir $(piq)_2$ (acac) (98:2)/bFPC:POT2T (1-1)	3.4	6381	6.5	2.9	(0.311; 0.424)	76	5654
B2	TFB:Ir $(piq)_2$ (acac) (98:2)/bTfPC:POT2T (1-1)	3.4	7513	4.8	2.1	(0.327; 0.471)	78	5625
A5	TFB:Ir $(piq)_2$ (acac) (95:5)/bFPC:POT2T (1-1)	4.2	8980	11.6	6.3	(0.384; 0.399)	92	3655
B5	TFB:Ir $(piq)_2$ (acac) (95:5)/bTfPC:POT2T (1-1)	4.5	7647	7.3	3.7	(0.396; 0.452)	89	3538
A10	TFB:Ir $(piq)_2$ (acac) (90:10)/bFPC:POT2T (1-1)	4.6	2986	5.8	2.6	(0.331; 0.516)	60	5080
B10	TFB:Ir $(piq)_2$ (acac) (90:10)/bTfPC:POT2T (1-1)	4.2	4761	3.8	1.7	(0.316; 0.415)	83	5461

[a] Turn-on voltage at luminance of 10 cd m^{-2}.
[b] Maximum brightness.
[c] Maximum current efficiency.
[d] Maximum external quantum efficiency.
[e] Commission Internationale de l'Eclairage (CIE) 1931 colour coordinates.
[f] Colour rendering index.
[g] Colour temperature (CIE, CRI and T_C values are related to EL spectra recorded at 9 V).

holes and electrons was mainly situated in the light-emitting layers (EML1), thus in the layers of **bFPC**:PO-T2T or **bTfPC**:PO-T2T. In the hole-transporting layer of TFB doped by Ir $(piq)_2$ (acac) of low concentration that additionally acted as the second light-emitting layer (EML2), hole and electron recombination was practically not expected because of high energy barrier (1.2 eV) for electrons on TFB/PO-T2T interface and due to favourable hole-transporting properties of compounds **bFPC** and **bTfPC** (Fig. 1c). According to this approach, hole and electron recombination on the low-energy emitter Ir $(piq)_2$ (acac) was prevented. Contribution of red phosphorescence from Ir $(piq)_2$ (acac) in devices A and B is expected when triplet excitons generated in EML1 either reach EML2 or recombination of holes and electrons occurs directly in EML2.

EL spectra of devices A and B were characterized by the bands related to the emissions of the different intensities of emitters Ir $(piq)_2$ (acac), **bFPC**:PO-T2T or **bTfPC**:PO-T2T and TFB (Fig. 4c). The most intensive green exciplex emission was detected for devices A2 and B2 with the lowest concentration of Ir $(piq)_2$ (acac). Apparently, blue TFB emission was caused by direct recombination of holes and electrons in EML2 and red Ir $(piq)_2$ (acac) emission resulted from diffusion of triplet excitons from EML1 to EML2. This consideration is supported by stable EL spectra of devices A and B at different external voltages (Fig. 4c). This observation indicates that charge disbalance practically did not occurr in the device structure due to the shift of charge-recombination zone from EML1 to EML2 with increasing applied voltages. With the increase of

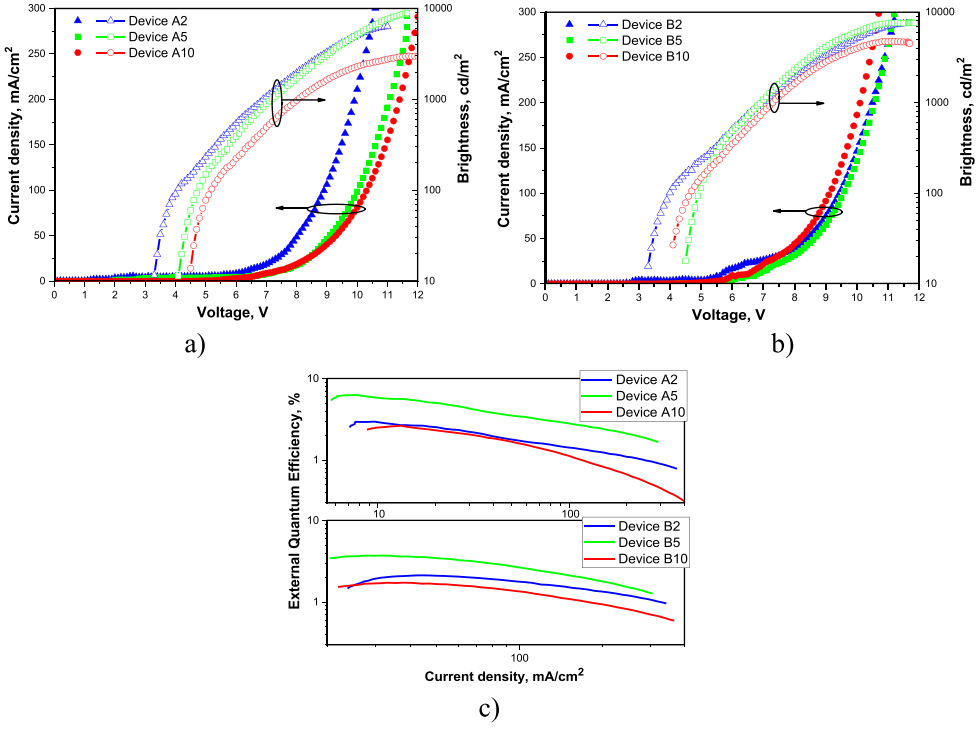

Fig. 5 – Current density/brightness versus applied voltage (a, b), external quantum efficiency versus current density (c) for the studied OLEDs.

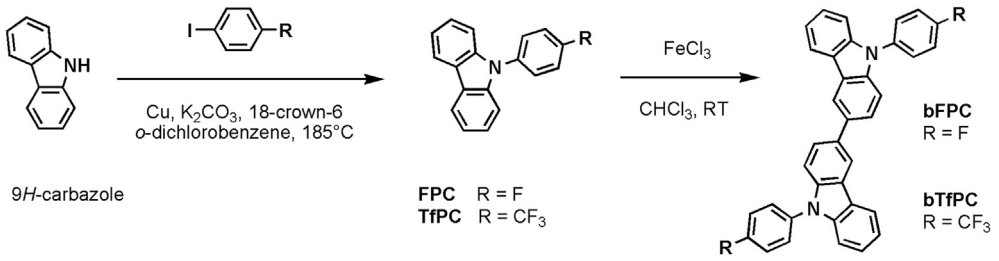

Scheme 1 – The synthetic path to fluoro- and trifluoromethyl-substituted 9,9′-diphenyl-3,3′-bicarbazole derivatives.

concentration of Ir $(piq)_2$ (acac) from 2 to 5%, the most intensive red phosphorescence was detected for devices A5 and B5. The increase of concentration of Ir $(piq)_2$ (acac) to 10% lead to the decrease of intensity of red phosphorescence which apparently was related to quenching of emission due to the triplet–triplet annihilation at high concentration of the emitter [46].

The highest colour rendering index (CRI) of 92 was observed for device A5 demonstrating the best combination of intensities of blue, green and red emissions in its EL spectrum with CIE1931 coordinates of (0.384, 0.399) and colour temperature (T_C) of 3655 K attributed to warm white light. The value of CRI is among the best values for white OLEDs [47,48]. Due to the broad emission spectra of the studied exciplexes and contribution of blue emission of TFB and red phosphorescence of Ir $(piq)_2$ (acac) to EL spectra of devices A and B, their CRI values are relatively high (Table 3).

Current density and brightness versus voltage curves are given in Fig. 5a, b. The efficient injection of charge carriers from electrodes and the following transport to emitting layers is confirmed by the low turn-on voltages (3.4–4.6 V) of all the fabricated OLEDs (Table 3). In addition to high quality of white colour of electroluminescence, high EQEs were observed for devices A5 and B5 due to the efficient triplet harvesting on two exciplex-based TADF emitters (**bFPC**:PO-T2T or **bTfPC**:PO-T2T) and phosphorescent emitter Ir $(piq)_2$ (acac). The highest maximum power, current, and quantum efficiencies of respectively 5.5 l m/W, 11.6 cd/A and 6.3% were observed for device A5 (Fig. 5c, Table 2). This device also showed the highest brightness of ca. 9000 cd/m^2 at 11.5 V.

4. Conclusions

Using the newly synthesized diphenyl bicarbazoles substituted by electron withdrawing fluoro- or trifluoromethylphenyl units as exciplex-forming donors and 2,4,6-tris [3-(diphenylphosphinyl)phenyl]-1,3,5-triazine as exciplex-forming acceptor, exciplex-forming emitters with efficient thermally activated delayed fluorescence were obtained. Exciplex-forming molecular mixture containing fluoro-substituted diphenyl bicarbazole demonstrated good performance in OLEDs mainly due to high hole mobility of $1.1 \cdot 10^{-3}$ cm^2/V·s at $1.6 \cdot 10^5$ V/cm of and lower activation energy of emission of 52 meV. The newly developed exciplex-forming systems were applied as active components of white hybrid electroluminescent diodes. The devices demonstrated high external quantum efficiency of 6.3% as for solution processable white OLEDs. High quality of warm-white electroluminescence with colour rendering index of 92, colour temperature of 3655 K and CIE1931 coordinates of (0.384, 0.399) was relatively stable under different voltages.

Declaration of Competing Interest

The authors declare that they have no known competing financial interests or personal relationships that could have appeared to influence the work reported in this paper.

Acknowledgement

This research was funded by European Union's Horizon 2020 research and innovation programme under the Marie Skłodowska-Curie Research and Innovation Staff Exchange (RISE) scheme (grant agreement No 823720).

Appendix ASupplementary data

Supplementary data to this article can be found online at https://doi.org/10.1016/j.jmrt.2020.12.058.

REFERENCES

[1] Sarma M, Wong KT. ACS Appl Mater Interfaces 2018;10:19279–304.
[2] Lee JH, Chen CH, Lee PH, Lin HY, Leung MK, Chiu TL, et al. J Mater Chem C 2019;7:5874–88.
[3] Goushi K, Yoshida K, Sato K, Adachi C. Nat Photon 2012;6:253–8.
[4] Jankus V, Data P, Graves D, McGuinness C, Santos J, Bryce MR, et al. Adv Funct Mater 2014;24:6178–86.
[5] Chen D, Liu K, Gan L, Liu M, Gao K, Xie G, et al. Adv Mater 2016;28:6758–65.
[6] Wei X, Liu Y, Hu T, Li Z, Liu J, Wang R, et al. Front Chem 2019;7.
[7] Regnat M, Pernstich KP, Kim KH, Kim JJ, Nüesch F, Ruhstaller B. Adv Electron Mater 2020;6:1–8.
[8] Nakanotani H, Furukawa T, Morimoto K, Adachi C. Sci Adv 2016;2:1–8.
[9] Pu YJ, Koyama Y, Otsuki D, Kim M, Chubachi H, Seino Y, et al. Chem Sci 2019;10:9203–8.
[10] Feng D, Dong D, Lian L, Wang H, He G. Org Electron 2018;56:216–20.

[11] Moon CK, Huh JS, Kim JM, Kim JJ. Chem Mater 2018;30:5648–54.
[12] Chapran M, Pander P, Vasylieva M, Wiosna-Salyga G, Ulanski J, Dias FB, et al. ACS Appl Mater Interfaces 2019;11:13460–71.
[13] Zhang M, Liu W, Zheng CJ, Wang K, Shi YZ, Li X, et al. Adv Sci 2019;6.
[14] Zhang D, Song X, Gillett AJ, Drummond BH, Jones STE, Li G, et al. Adv Mater 2020;32:1–9.
[15] Kreiza G, Banevičius D, Jovaišaitė J, Maleckaitė K, Gudeika D, Volyniuk D, et al. J Mater Chem C 2019;7:11522–31.
[16] Bunzmann N, Weissenseel S, Kudriashova L, Gruene J, Krugmann B, Grazulevicius JV, et al. Mater Horizons 2020;7:1126–37.
[17] Kim KH, Yoo SJ, Kim JJ. Chem Mater 2016;28:1936–41.
[18] Sasabe H, Toyota N, Nakanishi H, Ishizaka T, Pu YJ, Kido J. Adv Mater 2012;24:3212–7.
[19] Shih C-J, Lee C-C, Yeh T-H, Biring S, Kesavan KK, Al Amin NR, et al. ACS Appl Mater Interfaces 2018;10:24090–8.
[20] Al Amin NR, Kesavan KK, Biring S, Lee C-C, Yeh T-H, Ko T-Y, et al. ACS Appl Electron Mater 2020;2:1011–9.
[21] Kalinowski J. Mater Sci Pol 2009;27:735–56.
[22] Hung WY, Chi LC, Chen WJ, Chen YM, Chou SH, Wong KT. J Mater Chem 2010;20:10113–9.
[23] Duan L, Qiao J, Sun Y, Qiu Y. Adv Mater 2011;23:1137–44.
[24] Zieger SE, Steinegger A, Klimant I, Borisov SM. ACS Sens 2020;5:1020–7.
[25] Tonge CM, Paisley NR, Polgar AM, Lix K, Algar WR, Hudson ZM. ACS Appl Mater Interfaces 2020;12:6525–35.
[26] Gauthier S, Fréchet JMJ. Synth Met 1987:383–5.
[27] Vaitkeviciene V, Grigalevicius S, Grazulevicius JV, Jankauskas V, Syromyatnikov VG. Eur Polym J 2006;42:2254–60.
[28] Mallick S, Maddala S, Kollimalayan K, Venkatakrishnan P. J Org Chem 2019;84:73–93.
[29] Bredas JL. Mater Horizons 2014;1:17–9.
[30] Arkhipov VI, Fishchuk II, Kadashchuk A, Bässler H. .. In: Photophysics mol. Mater. Weinheim, FRG: Wiley-VCH Verlag GmbH & Co. KGaA; 2006. p. 261–366.
[31] Ivaniuk K, Cherpak V, Stakhira P, Hotra Z, Minaev B, Baryshnikov G, et al. J Phys Chem C 2016;120:6206–17.
[32] Lin TC, Sarma M, Chen YT, Liu SH, Lin KT, Chiang PY, et al. Nat Commun 2018;9:1–8.
[33] Sych G, Guzauskas M, Volyniuk D, Simokaitiene J, Starykov H, Grazulevicius JV. J Adv Res 2020;24:379–89.
[34] Galievsky VA, Druzhinin SI, Demeter A, Mayer P, Kovalenko SA, Senyushkina TA, et al. J Phys Chem A 2010;114:12622–38.
[35] Rettig W, Zander M. Chem Phys Lett 1982;87:229–34.
[36] Brunner K, Van Dijken A, Börner H, Bastiaansen JJAM, Kiggen NMM, Langeveld BMW. J Am Chem Soc 2004;126:6035–42.
[37] Holmes RJ, Forrest SR, Tung YJ, Kwong RC, Brown JJ, Garon S, et al. Appl Phys Lett 2003;82:2422–4.
[38] Han C, Zhang Z, Ding D, Xu H. Inside Chem 2018;4:2154–67.
[39] Nikolaenko AE, Cass M, Bourcet F, Mohamad D, Roberts M. Adv Mater 2015;27:7236–40.
[40] Yamazaki M. J Mol Catal A Chem 2004;213:81–7.
[41] Wu YC, Yang XF, Hao L. Sensor Actuator B Chem 2017;244:1113–20.
[42] Carraway ER, Demas JN, DeGraff BA, Bacon JR. Anal Chem 1991;63:337–42.
[43] Sekine C, Tsubata Y, Yamada T, Kitano M, Doi S. Sci Technol Adv Mater 2014;15.
[44] Su YJ, Huang HL, Le Li C, Chien CH, Tao YT, Chou PT, et al. Adv Mater 2003;15:884–8.
[45] Arias AC, MacKenzie JD, McCulloch I, Rivnay J, Salleo A. Chem Rev 2010;110:3–24.
[46] Giebink NC, D'Andrade BW, Weaver MS, MacKenzie PB, Brown JJ, Thompson ME, et al. J Appl Phys 2008;103.
[47] Jou JH, Chou YC, Shen SM, Wu MH, Wu PS, Lin CR, et al. J Mater Chem 2011;21:18523–6.
[48] Miao Y, Wang K, Zhao B, Gao L, Tao P, Liu X, et al. Nanophotonics 2018;7:295–304.